# Beating patterns of filaments in viscoelastic fluids

Henry C. Fu,[1,*] Charles W. Wolgemuth,[2,†] and Thomas R. Powers[1,‡]

[1]*Division of Engineering, Brown University, Providence, Rhode Island 02912, USA*
[2]*Department of Cell Biology, University of Connecticut Health Center, Farmington, Connecticut 06030, USA*

Many swimming microorganisms, such as bacteria and sperm, use flexible flagella to move through viscoelastic media in their natural environments. In this paper we address the effects a viscoelastic fluid has on the motion and beating patterns of elastic filaments. We treat both a passive filament which is actuated at one end and an active filament with bending forces arising from internal motors distributed along its length. We describe how viscoelasticity modifies the hydrodynamic forces exerted on the filaments, and how these modified forces affect the beating patterns. We show how high viscosity of purely viscous or viscoelastic solutions can lead to the experimentally observed beating patterns of sperm flagella, in which motion is concentrated at the distal end of the flagella.

## I. INTRODUCTION

Eukaryotes use beating cilia and flagella to transport fluid and swim [1]. Cilia and flagella share a common structure, consisting of a core axoneme of nine doublet microtubules arranged around two inner microtubules. Molecular motors slide the microtubule doublets back and forth to generate the observed beating patterns. Cilia typically have an asymmetric beating pattern, with a power stoke in which the extended cilium pivots about its base, and a recovery stroke in which the cilium bends sharply as it returns to its position at the beginning of the cycle [2]. This stroke pattern is effective for moving fluid past the body of the cell, such as the epithelial cells of the airway or the surface of a swimming *Paramecium*. On the other hand, flagella typically have a symmetric planar or helical wave form [2], such as the flagellum of bull sperm which exhibits a traveling wave with an amplitude that increases with distance from the head of the sperm [3]. The shape of the centerline of a beating filament determines the rate of transport or swimming. Many studies show that this shape depends on the properties of the medium. For example, the flagella of human sperm have a slightly helical wave form in water. As viscosity increases via the addition of polymers, the wave form becomes less helical and the amplitude flattens along most of the flagellum, with all the deflection taking place at the free end [4] (Fig. 1). Similar effects are observed in cervical mucus and other viscoelastic solutions [3,5].

In this paper, we calculate the shape of a beating filament as a function of the properties of the medium. Since the size scale for the filaments is tens of microns, and since typical swimming speeds are tens to hundreds of microns per second, the Reynolds number is very small, and inertia is unimportant. The medium is modeled with a single-relaxation time fading-memory model for a polymer solution [6]. We consider two different models for the filament. First, we con-

sider the passive case, in which one end of a flexible filament is waved up and down [7–10]. We also consider a more realistic active model in which undulations arise from internal sliding forces distributed all along the length of the filament [11,12]. Although active filaments are a closer representation of eukaryotic flagella, we show that many of the important features of swimming filaments in viscoelastic media are also present in the simple passive filament. Furthermore, passive filaments may be more amenable to experiment and quantitative comparison with theory. Our main results are qualitative explanations for some of the beating shapes observed in sperm in high-viscosity and viscoelastic solutions [3–5,13,14]. These results indicate that the observed shape change with increasing viscosity is a physical rather than a behavioral response. We reported some of our results for the case of an active filament in a viscoelastic medium with zero solvent viscosity in a previous publication [15]. In addition to presenting interesting results for the passive filament in a viscoelastic medium, in the present paper we also systematically study the dependence of the shape of an active filament on solvent viscosity.

To make the analysis as simple as possible, we work to linear order in the deflection of the filament away from a straight configuration. Although the power dissipated by a beating filament is second order in deflection, it is sufficient to calculate the shape to first order in deflection to accurately compute the power to second order. We calculate how this power varies as the beating pattern changes with increasing relaxation time. There are also important changes in the swimming velocity due to shape change. Even in a linearly



FIG. 1. The wave form of a human sperm observed by Ishijima *et al.* [4] in a solution with very high viscosity (400 cP). The sperm head, on the left side of the image, is held in place with a micropipette tip. The contour length of the flagellum is approximately 40 $\mu$m.

*Henry_Fu@brown.edu
†cwolgemuth@uchc.edu
‡Thomas_Powers@brown.edu

viscoelastic fluid, for which the swimming speed of a filament with prescribed beating pattern is the same as in a Newtonian fluid [16], changes to the beating patterns due to the viscoelastic response can lead to changes in swimming velocities. However, as has been previously emphasized [15,17], in viscoelastic fluids the swimming velocity also receives corrections from the nonlinearity of the fluid constitutive relation at second order, and both these nonlinear corrections and the changes to the beating patterns must be taken into account to correctly calculate the swimming velocity [15].

We begin our analysis by reviewing commonly used theories for the internal forces acting on passive and active filaments. Then we introduce the Oldroyd-B fluid, the fading-memory model we will use throughout this paper. After providing context with a brief discussion of resistive force theory for Newtonian viscous fluids, we discuss resistive force theory for small amplitude motions of a slender filament in an Oldroyd-B fluid. Using the balance of internal and external forces, we calculate the shape of a beating filament for both the passive and active cases. We close the main text with a discussion of the limitations of our analysis and the implications of our results. In the Appendix, we discuss further the subtleties of applying linear viscoelasticity to the swimming problem. There we show that linear viscoelastic constitutive relations lead to incorrect predictions for the case of an active filament in a rotating viscoelastic medium.

## II. MODELS

### A. Internal forces acting on flexible filaments

The internal forces acting on a filament may be specified either by the energy as a function of the curvature or a constitutive relation for the moment acting on a cross section of the filament. The two approaches are equivalent, and in this paper we use the moment on a cross section.

#### 1. Passive filament

We first consider the passive elastic filament. Let $\mathbf{r}(s)$ denote the path of the centerline of an inextensible filament of length $L$. Then the moment $\mathbf{M}$ due to internal stresses acting on the cross section of a bent filament is

$$\mathbf{M} = A\mathbf{r}' \times \mathbf{r}'', \qquad (1)$$

where $A$ is the bending modulus and primes denote differentiation with respect to $s$ [18]. Since we only consider planar filaments in this paper, it is convenient to introduce the right-handed orthonormal frame $\{\hat{\mathbf{e}}_1, \hat{\mathbf{e}}_2, \hat{\mathbf{e}}_z\}$, where $\hat{\mathbf{e}}_1 = \mathbf{r}'$ is the tangent vector of $\mathbf{r}(s)$, and $\hat{\mathbf{e}}_z$ is normal to the plane of the filament. Thus $\kappa = \hat{\mathbf{e}}_2 \cdot \hat{\mathbf{e}}_1'$ is the curvature of the the curve $\mathbf{r}(s)$. Note that the sign of $\kappa$ is meaningful since $\hat{\mathbf{e}}_2$ does not flip at inflection points. Throughout this paper, we use a coordinate system for which the straight filament lies in the $\hat{\mathbf{e}}_x$ direction, and consider only planar motion of the filament in the $\hat{\mathbf{e}}_x$-$\hat{\mathbf{e}}_y$ plane. Further, we restrict ourselves to small displacements of the filament, so that $\mathbf{r}(s) \approx s\hat{\mathbf{e}}_x + h(s)\hat{\mathbf{e}}_y$. For such small displacements, we may approximate $\kappa \approx h''$ and $\mathbf{M} \approx \hat{\mathbf{e}}_z A h''$. The elastic force per unit length on the filament is found by moment balance,
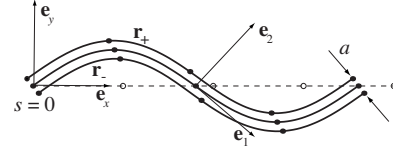


FIG. 2. Sliding filament model. The dotted line is the centerline of the flagellum when it is straight; the circles divide it in quarters. The solid lines represent the bent centerline and $\mathbf{r}_\pm$; the dots divide each line in quarters as measured along the respective contours. All three curves have length $L$.

$$\mathbf{M}' + \hat{\mathbf{e}}_1 \times \mathbf{F} = 0, \qquad (2)$$

where $\mathbf{F}$ is the force acting on a cross section at $s$. For small displacements, the force per unit length due to internal stresses is therefore $\mathbf{f}_{\text{int}} = \mathbf{F}' \approx -Ah''''\hat{\mathbf{e}}_y$. Equation (2) also allows a tangential force that may be identified as a tension. For small displacements, the tension force is higher order in displacements than the normal forces, and so we ignore it in this work [19]. In the small Reynolds number flows associated with swimming cells, the total force on each element of the filament must be zero, $\mathbf{f}_{\text{ext}} + \mathbf{f}_{\text{int}} = 0$. As we shall see below, the leading order shape of the filament is determined by external forces which are linear in the velocity of the filament elements, even in nonlinearly viscoelastic fluids. Therefore force balance yields a fourth order linear differential equation to be solved for the time-dependent filament shape.

The differential equation must be supplemented with appropriate boundary conditions. For the free end, we have

$$-Ah'''(L) = 0, \qquad (3)$$

$$Ah''(L) = 0, \qquad (4)$$

corresponding to zero force and torque, respectively. For the driven end, we may consider prescribed angle,

$$h'(0) = \epsilon \cos(\omega t), \qquad (5)$$

$$h(0) = 0, \qquad (6)$$

or prescribed force

$$-Ah'''(0) = \epsilon \cos(\omega t), \qquad (7)$$

$$h(0) = 0. \qquad (8)$$

#### 2. Active filament

For a simple model of a sperm flagellum which incorporates active bending forces, we consider a swimmer consisting of a flagellum which always lies in the plane, and disregard the presence of a head. We model the flagellum as two inextensible filaments of length $L$ which are parallel and have a fixed, uniform separation $a$. The filaments can slide past each other, which causes the flagellum to bend (Fig. 2). Define the paths of the two filaments as

$$\mathbf{r}_\pm = \mathbf{r} \pm (a/2)\hat{\mathbf{e}}_2, \qquad (9)$$

where the frame $\{\hat{\mathbf{e}}_1, \hat{\mathbf{e}}_2, \hat{\mathbf{e}}_z\}$ again applies to the centerline $\mathbf{r}(s)$ of the filament (Fig. 2). Equation (9) implies $ds_+ - ds_-$

$= -a\kappa ds$, where $s_\pm(s)$ is the arclength of $\mathbf{r}_\pm(s)$. For example, $\kappa < 0$ in the interval $0 < s < L/2$ of the curve $\mathbf{r}$ in Fig. 2. Thus the arclength $s_+(L/2)$ of $\mathbf{r}_+(s)$ is *longer* than $L/2$; likewise, the arclength $s_-(L/2)$ is shorter than $L/2$. In the region $0 < s < L/2$, the material points of $\mathbf{r}_+$ have slid backwards relative to the material points of $\mathbf{r}_-$. Integrating $ds_+ - ds_-$, we find that the distance filament $\mathbf{r}_-$ slides past filament $\mathbf{r}_+$ at $s$ is

$$\Delta(s) = -\int_0^s a\kappa(s)ds = -a[\theta(s) - \theta(0)], \qquad (10)$$

where $\theta$ is the angle between $\hat{\mathbf{e}}_1$ and $\hat{\mathbf{e}}_x$. Note that Eq. (10) is exact, although from here on we assume $a\kappa \ll 1$.

The composite filament is actuated by molecular motors that slide $\mathbf{r}_\pm$ back and forth past each other. Let $f_m$ denote the force per unit length in the $\hat{\mathbf{e}}_1$ direction that the upper filament $\mathbf{r}_+$ exerts on the lower filament $\mathbf{r}_-$ through the motors. To first order in deflection, the total moment acting across the cross section at $s$ is therefore given by

$$M_z = Ah''(s) + a\int_s^L f_m(s)ds. \qquad (11)$$

In this model, the bending modulus $A$ is an effective modulus representing the stiffness of the entire flagellar structure. We note that there are additional forces that may be included in modeling eukaryotic flagella, such as those arising from linking proteins that resist the sliding of filaments past each other. In this work we leave those out for simplicity; we have found that for reasonable magnitudes of these forces they do not change our results qualitatively. Moment balance, Eq. (2), applies as before, leading to a force on the cross section at $s$ of $\mathbf{F} = (-Ah''' + af_m)\hat{\mathbf{e}}_y$, or an internal force per unit length of $\mathbf{f}_{int} = (-Ah'''' + af_m')\hat{\mathbf{e}}_y$.

The boundary conditions for the active filament involve extra terms from the sliding force. At the free end, zero force and moment give

$$-Ah'''(L) + af_m(L) = 0, \qquad (12)$$

$$Ah''(L) = 0. \qquad (13)$$

At the attachment to the head we may consider a variety of situations. For a fixed head, we may consider clamped and hinged boundary conditions. For clamped boundary conditions,

$$h(0) = 0, \qquad (14)$$

$$h'(0) = 0. \qquad (15)$$

For hinged boundary conditions where the total moment vanishes,

$$Ah''(0) + a\int_0^L f_m(s)ds = 0, \qquad (16)$$

$$h(0) = 0. \qquad (17)$$

### B. Linearly and nonlinearly viscoelastic fluids

In the limit of zero Reynolds number, the equation of motion of an incompressible medium is given by force balance, $-\nabla p + \nabla \cdot \boldsymbol{\tau} = 0$, where $p$ is the pressure enforcing incompressibility, $\nabla \cdot \mathbf{v} = 0$; $\mathbf{v}$ is the velocity; and $\boldsymbol{\tau}$ is the deviatoric stress tensor.

The material properties of the medium are given by the constitutive relation, which specifies the stress in the medium as a function of the strain and strain history of the material. In a Newtonian fluid with viscous forces, the stress tensor is proportional to the rate of strain. In contrast, in a viscoelastic fluid, there is an additional elastic component to the response of the medium. This effect is incorporated by fading-memory models, in which the stress relaxes over time to the viscous stress. We will focus on a particular fading-memory model, the Oldroyd-B fluid, which has the constitutive relation

$$\boldsymbol{\tau} + \lambda\overset{\triangledown}{\boldsymbol{\tau}} = \eta\dot{\boldsymbol{\gamma}} + \lambda\eta_s\overset{\triangledown}{\dot{\boldsymbol{\gamma}}}. \qquad (18)$$

In this equation, $\lambda$ is the single relaxation time, $\overset{\triangledown}{\boldsymbol{\tau}} = \partial_t\boldsymbol{\tau} + \mathbf{v}\cdot\nabla\boldsymbol{\tau} - (\nabla\mathbf{v})^\mathsf{T}\cdot\boldsymbol{\tau} - \boldsymbol{\tau}\cdot\nabla\mathbf{v}$ is the upper-convected time derivative of $\boldsymbol{\tau}$, $\mathbf{v}$ is the velocity, $\eta$ is the polymer viscosity, $\dot{\boldsymbol{\gamma}} = \nabla\mathbf{v} + (\nabla\mathbf{v})^\mathsf{T}$ is the strain rate, and $\overset{\triangledown}{\boldsymbol{\gamma}}$ is the upper-convected time derivative of the strain rate. In this paper we will use a dot to denote time differentiation. The total viscosity $\eta = \eta_p + \eta_s$ is the sum of polymer and solvent viscosities. The Oldroyd-B fluid is one of the simpler nonlinear constitutive relations for a viscoelastic fluid. The upper-convected time derivative is the source of nonlinearities [6]. If the solvent viscosity is ignored ($\eta_s = 0$), the Oldroyd-B fluid reduces to the upper convected Maxwell fluid, and if there is no polymer ($\eta = \eta_s$) the Oldroyd-B fluid reduces to a Newtonian fluid. The Oldroyd-B fluid is known to describe elastic and first normal stress effects as long as elongational flows are not large; however, it does not capture shear-thinning or yield-stress behaviors observed in some non-Newtonian fluids.

Although we have introduced the nonlinearly viscoelastic fluid, in what follows we will only work to linear order in the displacements of filaments. In that case, our results will be the same as if we consider the same model with ordinary time derivatives, which corresponds to a linear Maxwell-Kelvin fluid.

### III. FILAMENTS IN NEWTONIAN FLUIDS

The motion and swimming properties of filaments in Newtonian fluids have been actively studied by many researchers [7,8,10,11]. Here we briefly summarize results in the Newtonian case which will be useful for comparison to filaments in viscoelastic fluids.

A common approach to calculating the viscous forces acting on a flagellum is resistive force theory, a local drag theory in which the forces per unit length acting on a thin filament are proportional to the fluid velocity relative to the filament [20]. Although resistive force theory does not completely capture the effects of hydrodynamic interactions, macroscopic-scale experiments have shown that it is surprisingly accurate for single filaments [9,21,22]. For a purely

viscous liquid, the force per unit length acting on a filament moving in an otherwise quiescent fluid is given by

$$\mathbf{f}_{\text{vis}} = -\zeta_{\parallel}(\hat{\mathbf{e}}_1 \cdot \dot{\mathbf{r}})\hat{\mathbf{e}}_1 - \zeta_{\perp}(\hat{\mathbf{e}}_2 \cdot \dot{\mathbf{r}})\hat{\mathbf{e}}_2, \qquad (19)$$

where the friction coefficients $\zeta_{\parallel}$ and $\zeta_{\perp}$ depend weakly on the filament radius, are proportional to the viscosity $\eta$, and satisfy $\zeta_{\perp} \approx 2\zeta_{\parallel}$.

For simplicity, assume that there is only one frequency of motion for the filament, so the displacement of the filament can be written $h(s,t) = \text{Re}\{\tilde{h}(s,t)\exp(-i\omega t)\}$. In this case, using the resistive force theory, the $y$ component of the equation of motion for the passive and active filament are, respectively,

$$-i\omega\zeta_{\perp}\tilde{h} = -A\tilde{h}'''', \qquad (20)$$

$$-i\omega\zeta_{\perp}\tilde{h} = -A\tilde{h}'''' + a\tilde{f}_{\text{m}}', \qquad (21)$$

where $f_{\text{m}} = \text{Re}\{\tilde{f}_{\text{m}}(s)\exp(-i\omega t)\}$. The solutions of these can be obtained in a manner similar to that described in Sec. V to give $h(s,t)$.

From $h(s,t)$, we may calculate the power dissipated by the filament and the swimming velocity of the filament. At each material element of the filament, the power dissipated is the inner product of the hydrodynamic force and the velocity. The total time-averaged power dissipated is therefore

$$\langle P \rangle = \frac{\zeta_{\perp}\omega^2}{2}\int_0^L ds|\tilde{h}(s)|^2. \qquad (22)$$

The swimming velocity can be determined by the constraint under Stokes flow that the total force on the swimmer is zero. To lowest order, the component of force in the $\hat{\mathbf{e}}_y$ direction is zero as a result of the equation of motion for the filament shape. The beating motion of the filament produces a $\hat{\mathbf{e}}_x$ component of the time-averaged force that is second order in the deflection, which is balanced by a drag force from overall translation, i.e., swimming with velocity $U_{\text{RFT}}$ in the $\hat{\mathbf{e}}_x$ direction:

$$U_{\text{RFT}} = \frac{\omega(\zeta_{\perp} - \zeta_{\parallel})}{2L\zeta_{\parallel}}\,\text{Im}\int_0^L ds\tilde{h}'\tilde{h}^*, \qquad (23)$$

where $\tilde{h}^*$ is the complex conjugate of $\tilde{h}$. In this paper we ignore the drag from the head, which would contribute an additional factor in the expression for $U_{\text{RFT}}$. Note that for clamped boundary conditions, the torque exerted on the filament at $s=0$ has a reaction torque that causes the head and ultimately the whole sperm to rotate [10]. Here we ignore these effects for two reasons: (i) Experiments looking at the shape of beating filaments can be performed with an immobilized head. (ii) For swimming, calculations ignoring the head are simpler and can be easily compared to previous work, e.g., [11], and also are more easily extended and compared to the calculations we will perform in the viscoelastic fluid.

It is important to note that it is only necessary to solve for the beating motion to first order in deflection amplitude to obtain the correct leading order results for the power and the swimming speed, even though these quantities are of second order in deflection.

## IV. FILAMENTS IN VISCOELASTIC FLUIDS

Having seen how to analyze filaments in Newtonian fluids, we turn to viscoelastic fluids. In a viscoelastic fluid, the hydrodynamic force felt by the filament is no longer given by Eq. (19). Due to the change in forces, the equations of motion for the filament are changed, so that the beating patterns change. Since both the beating patterns and forces affect the power dissipated and swimming velocity, we expect both of those to change as well. To calculate the power dissipated by a filament beating in a viscoelastic medium to leading order in the deflection, we only need the velocity and the force to first order. Thus it is sufficient to find the shape to first order. From Eq. (23) we expect that a change in the first-order shape $h$ will change the swimming velocity; however, there are additional second order corrections that are present even for a waveform of prescribed shape [15,17]. Consistency requires including both of these second order corrections [15]. In this paper we concentrate on the effects of viscoelasticity on beating patterns and power dissipated.

The calculation of the force per unit length acting on a slender filament undergoing large deflections in a viscoelastic fluid is a daunting challenge. Since we consider small deflections, we may consider the simpler problem of the forces per unit length acting on a slightly perturbed infinitely long cylinder with a prescribed lateral or longitudinal traveling wave. Elsewhere we solve for the flow induced by these motions using the Oldroyd-B fluid and calculate the forces acting on the deformed cylinder [23]. We find that the force per unit length $\mathbf{f}_{\text{Oldroyd}}$ obeys

$$\mathbf{f}_{\text{Oldroyd}} + \lambda_1\dot{\mathbf{f}}_{\text{Oldroyd}} = \mathbf{f}_{\text{vis}} + \frac{\eta_s}{\eta}\lambda\dot{\mathbf{f}}_{\text{vis}}. \qquad (24)$$

In the limit of zero solvent viscosity, $\eta_s = 0$, Eq. (24) is the same as the resistive force theory proposed by Fulford, Katz, and Powell for the linear Maxwell model [16]. Equation (24) is valid for slender filaments and to first order in small deflections.

### Application to passive and active filaments

To apply the above results to the passive and active filament models, we use the hydrodynamic force $\mathbf{f}_{\text{Oldroyd}}$ in the equations of motion. For the passive filament with a single frequency of motion, we find

$$-i\omega\frac{1-i\text{De}_2}{1-i\text{De}}\zeta_{\perp}\tilde{h} = -A\tilde{h}'''', \qquad (25)$$

where the Deborah numbers $\text{De} = \omega\lambda$ and $\text{De}_2 = \text{De}\,\eta_s/\eta$. For the active filament we must include the motor forcing:

$$-i\omega\frac{1-i\text{De}_2}{1-i\text{De}}\zeta_{\perp}\tilde{h} = -A\tilde{h}'''' + a\tilde{f}_{\text{m}}'. \qquad (26)$$

The beating pattern is determined by solving these equations of motion, and once the beating pattern is known, the power

dissipated and swimming velocity can be calculated.

The power dissipated is calculated in the same way as for a Newtonian fluid, except that now the force per unit length is specified by Eq. (24), leading to

$$\langle P \rangle = \frac{\zeta_\perp \omega^2}{2} \frac{1 + \mathrm{De}\mathrm{De}_2}{1 + \mathrm{De}^2} \int_0^L ds |\tilde{h}(s)|^2. \tag{27}$$

As noted above, the beating pattern affects the swimming velocity. However, there is an additional correction to the swimming velocity in the nonlinearly viscoelastic Oldroyd-B fluid. Instead of Eq. (23), the correct expression for the swimming speed is [15,23]

$$U = \frac{1 + \mathrm{De}\mathrm{De}_2}{1 + \mathrm{De}^2} \left\langle \int_0^L ds\, h'(s,t) \dot{h}(s,t) \right\rangle \tag{28}$$

$$= \frac{1 + \mathrm{De}\mathrm{De}_2}{1 + \mathrm{De}^2} U_{\mathrm{RFT}}, \tag{29}$$

where the second line follows from the ratio $\zeta_\perp / \zeta_\parallel = 2$. This result applies to an infinite cylinder moving with beating pattern $h(s,t) = \mathrm{Re}\{\tilde{h}(s)\exp(-i\omega t)\}$. To apply this result to the finite filament, we imagine periodically replicating the calculated beating pattern of the filament so that it becomes infinitely long. Although this construction generally leads to an infinite filament with discontinuities in $h(s,t)$ with spacing $L$, the swimming speed of such an infinite filament may be calculated using the Fourier-space version of Eq. (28), or, equivalently, by invoking the periodicity and performing the real-space integral from 0 to $L$. This result ignores end effects from the flow around the end of the finite filament. We have mentioned the effects of beating patterns on swimming velocity here for completeness. In the rest of the paper we focus on the changes to beating patterns themselves and power dissipation rather than swimming velocity.

## V. RESULTS

### A. Nondimensionalization

We can nondimensionalize the filament equations of motion and boundary conditions by measuring lengths in terms of $L$, $f_\mathrm{m}$ in terms of $A/(aL^2)$, and time in terms of $\omega^{-1}$. Velocities are measured in terms of $L\omega$ and angular velocities in terms of $\omega$. For notational simplicity, after scaling we use the same symbols for the new quantities. The nondimensional equation of motion for the passive filament with a single frequency is

$$-i\mathrm{Sp}^4 \frac{1 - i\mathrm{De}_2}{1 - i\mathrm{De}} \tilde{h} + \tilde{h}'''' = 0, \tag{30}$$

with boundary conditions

$$-h'''(1) = 0, \tag{31}$$

$$h''(1) = 0, \tag{32}$$

$$h(0) = 0, \tag{33}$$

and either of

$$h'(0) = \epsilon \cos(t) \quad \text{(prescribed angle)}, \tag{34}$$

$$h'''(0) = \epsilon \cos(t) \quad \text{(prescribed force)}. \tag{35}$$

The dimensionless parameter $\mathrm{Sp} = L(\omega \zeta_\perp / A)^{1/4}$, known as the sperm number, involves the ratio of the bending relaxation time of the filament to the period of the traveling wave. In what follows the forcing $\epsilon$ is chosen small enough so that we remain safely in the linear regime.

The nondimensional equation of motion for the active filament with a fixed head and single frequency becomes

$$-i\mathrm{Sp}^4 \frac{1 - i\mathrm{De}_2}{1 - i\mathrm{De}} \tilde{h} + \tilde{h}'''' - \tilde{f}_\mathrm{m}' = 0, \tag{36}$$

where $f_\mathrm{m} = \mathrm{Re}\{\tilde{f}_\mathrm{m}(s)\exp(-it)\}$. The boundary conditions for Eq. (36) are

$$-h'''(1) + f_\mathrm{m}(1) = 0, \tag{37}$$

$$h''(1) = 0, \tag{38}$$

$$h(0) = 0, \tag{39}$$

and either of

$$h'(0) = 0 \quad \text{(clamped)}, \tag{40}$$

$$h''(0) + \int_0^1 f_\mathrm{m}(s)ds = 0 \quad \text{(hinged)}. \tag{41}$$

### B. Passive filament

For the passive filament with harmonic time dependence, we examine the solutions to Eq. (30) which are

$$h_\mathrm{h}(s) = \sum_{j=1}^4 C_j \exp(r_j s), \tag{42}$$

where the $r_j$ solve

$$-i\mathrm{Sp}^4 \frac{1 - i\mathrm{De}_2}{1 - i\mathrm{De}} + r_j^4 = 0. \tag{43}$$

The four coefficients $C_j$ are determined by the boundary conditions, and the full time-dependent solution is then given by

$$h(s,t) = \mathrm{Re}\{e^{-it} h_\mathrm{h}(s)\}. \tag{44}$$

From the form of $h_\mathrm{h}$ in Eq. (42), we can already make a general comment about the expected form of beating patterns. The exponentials in Eq. (42) will lead to traveling or standing waves. Standing waves can only form if there are pairs of $r_j$ that are complex conjugates, which happens only in the elastic limit ($\mathrm{De} \to \infty$), where the $r_j$ are proportional to $\pm(1 \pm i)$. Therefore in the viscous case the beating pattern will always have the form of a traveling wave, but as De increases the beating pattern takes on more characteristics of a standing wave.

Representative plots of these solutions for prescribed attachment angles and forces are presented in Fig. 3. Solutions
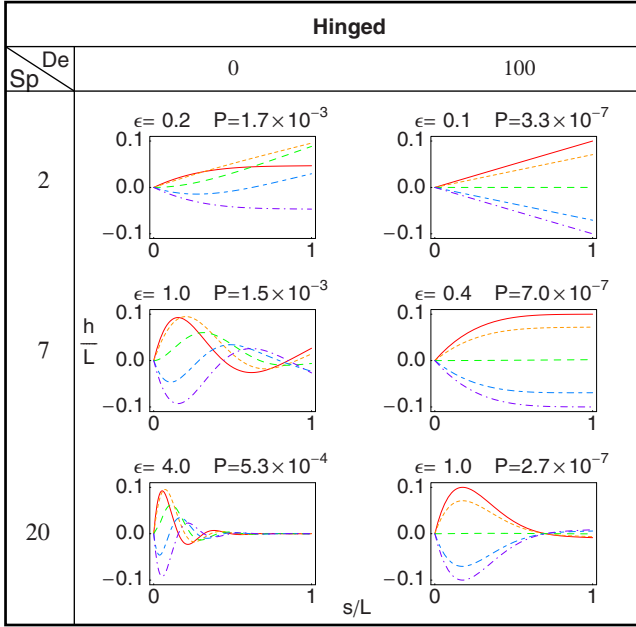
FIG. 3. (Color online) Shapes of beating patterns for passive filaments driven by prescribed angle at the left end ($s=0$). A half cycle of the pattern is shown for viscous (De=0) and viscoelastic (De=100) cases, and sperm number 2, 7, and 20. Time sequence: solid (red), short dash (orange), long dash (green), long dash-short dash (blue), dash-dot (purple). The ratio of solvent viscosity to the total viscosity is $\eta_s / \eta = \text{De}_2/\text{De} = 10^{-4}$. At the top of each plot, we print the (dimensionless) angular magnitude $\epsilon$ required to produce motion with amplitude $0.1L$, and the (dimensionless) power dissipated by the motion.

for the viscous (De=0) and viscoelastic (De=100) limits are plotted side by side. As expected, changing the viscoelastic character of the fluid by varying the Deborah number induces changes in the shapes of the beating patterns. An important feature of these solutions is the presence of a bending length scale $\xi$: $\xi/L = |r_j|^{-1} = \text{Sp}^{-1}|(1-i\text{De}_2)/(1-i\text{De})|^{-1/4}$. For De=0, the purely viscous case, $\xi$ is set by the sperm number alone; a stiff filament with small sperm number has large $\xi$ and acts as a rigid rod, while a flexible filament with large sperm number has small $\xi$ and can bend in response to viscous forces. Increasing the Deborah number acts to increase $\xi$. In Fig. 3, the amplitude of the prescribed driving angle is selected so that the maximum displacement of the filament is $L/10$, and then printed above each figure. The beating pattern is linear in the amplitude of the driving angle. Due to larger bending lengths, $\xi$, in viscoelastic fluids, smaller driving angles are typically required to produce the same amplitude motion.

The beating patterns in Fig. 3 also demonstrate that viscoelastic effects alter the nature of the beating patterns as expected from the form of Eq. (42): for De=0, we obtain traveling wave beating patterns, while for large De, in the elastic limit, we obtain standing wave beating patterns.

From Eq. (27) we find the time-averaged power dissipated

$$\langle P_M \rangle = \frac{\zeta_\perp}{2} \text{Re}\left[ \int_0^L ds\, \omega^2 |\tilde{h}|^2 \frac{1 - i\text{De}_2}{1 - i\text{De}} \right] \quad (45)$$
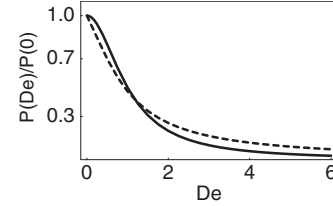


FIG. 4. Time-averaged power dissipated by passive filaments driven by prescribed angle, as a function of De=$\omega\lambda$ (dashed curve). Power is normalized to the power dissipated in the viscous case De=0. The black curve corresponds to the power dissipated if the beating pattern does not change from the viscous case, but the filament is placed in a viscoelastic medium. In both cases, Sp=7. The driving amplitude is chosen so that the maximum amplitude of the beating pattern is $L/10$ in the viscous case. The ratio of solvent viscosity to the total viscosity is $\eta_s / \eta = \text{De}_2/\text{De} = 10^{-4}$.

$$= \zeta_\perp \omega^2 \frac{1 + \text{De}\text{De}_2}{2(1 + \text{De}^2)} \int_0^L ds |\tilde{h}|^2. \quad (46)$$

The power dissipated by each beating pattern is printed above the images in Fig. 3. Note that the power dissipated is proportional to the beating amplitude squared, and hence also proportional to $\epsilon^2$. Figure 4 shows the power dissipation versus Deborah number (dashed curve) for Sp=7 and constant driving amplitude. We also display the power dissipation, Eq. (46), evaluated with the purely viscous (De=0) shape $\tilde{h}$ (solid curve). Note that the difference in shape $\tilde{h}$ between the viscous and viscoelastic cases has little effect. The power is mainly governed by the explicit factors of De in the relation between $\mathbf{f}_{\text{Oldroyd}}$ and $\mathbf{f}_{\text{vis}}$.

### C. Active filaments

#### 1. Fixed head

Examining Eq. (36), we find that it only differs from the passive case at the boundary conditions and by the presence of an inhomogeneous term. Therefore we may use the homogeneous solution from the previous subsection,

$$h_{\text{h}}(s) = \sum_{j=1}^{4} C_i \exp(r_j s), \quad (47)$$

and add to it a particular solution. As in the passive case, beating patterns with traveling waves are expected in the viscous limit, and increasing the Deborah number leads to beating patterns with characteristics of standing waves.

To find the particular solution, let us assume that the internal sliding force takes the form of a traveling wave

$$f_{\text{m}}(s) = \text{Re}\{\bar{f}_{\text{m}} \exp(iks - it)\}. \quad (48)$$

In that case, we can write the particular solution

$$h_{\text{p}} = ik\bar{f}_{\text{m}}e^{iks}/[-i\text{Sp}^4(1 - i\text{De}_2)/(1 - i\text{De}) + k^4]. \quad (49)$$

Again the four boundary conditions set the four unknown coefficients, and the full time-dependent solution is

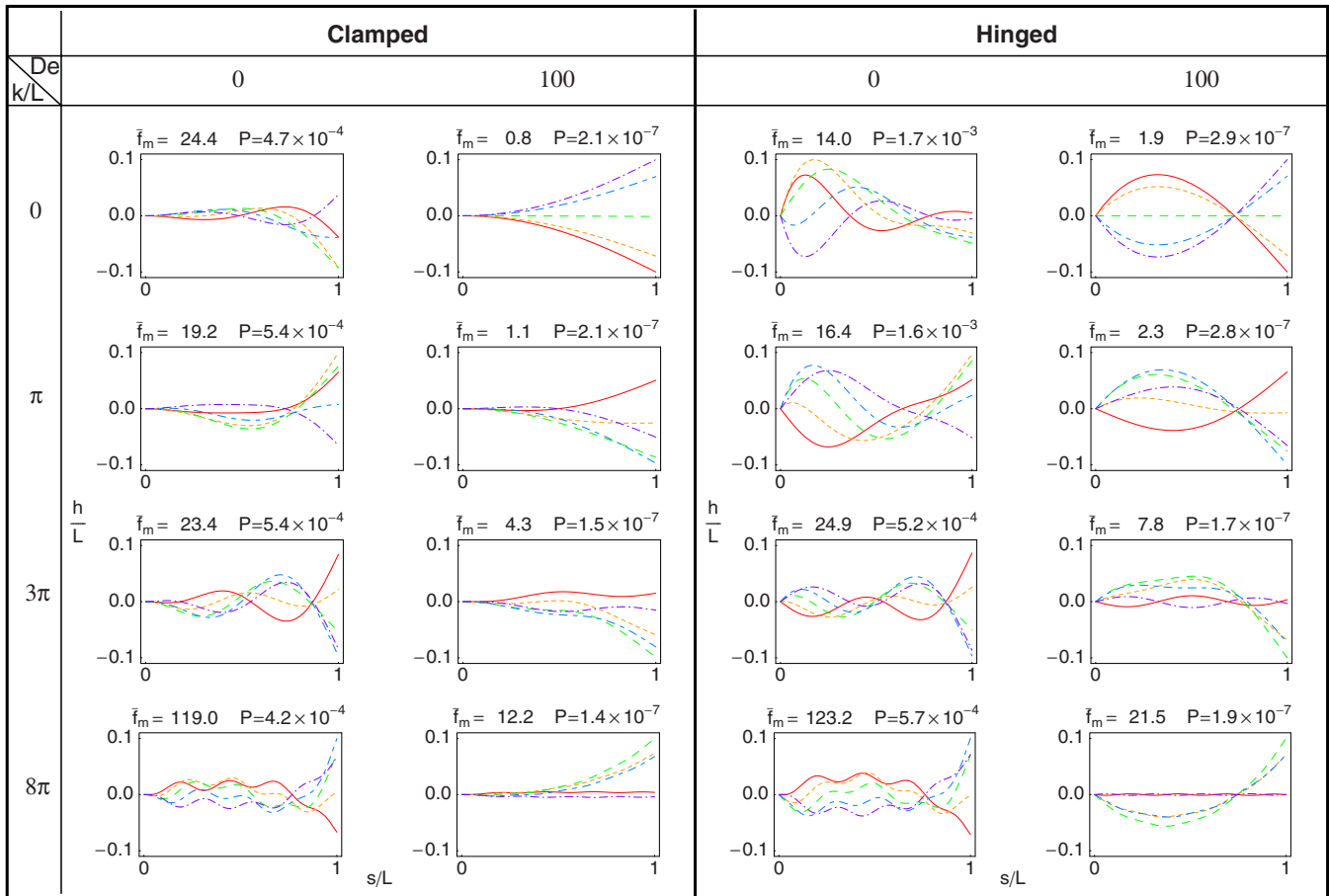$$h(s,t) = \text{Re}\{e^{-it}[h_{\text{h}}(s) + h_{\text{p}}]\}. \quad (50)$$

FIG. 5. (Color online) Shapes of beating patterns for filaments with internal sliding forces and fixed head position, with Sp=7. A half cycle of the pattern is shown for viscous (De=0) and viscoelastic (De=100) cases, and for internal sliding forces given by Eq. (48) with $k/L$ varying from 0 (uniform force) to $8\pi$, as indicated. Time sequence: solid (red), short dash (orange), long dash (green), long dash-short dash (blue), dash-dot (purple). At the top of each figure, we print the (dimensionless) magnitude $\bar{f}_m$ required to produce motion with amplitude $0.1L$, and the (dimensionless) power dissipated by the motion. The ratio of solvent viscosity to the total viscosity is $\eta_s/\eta = \mathrm{De}_2/\mathrm{De} = 10^{-4}$.

The beating shapes of the active flagellum and a fixed head are shown in Fig. 5, for De=0 (viscous case) and De =100 (viscoelastic case), and for various spatial dependencies of the internal sliding force. Similarly to the passive case, the beating amplitude is proportional to the driving force $\bar{f}_m$. The forces required to produce beating with amplitude $0.1L$ are larger in the viscous cases than the viscoelastic cases, again since the bending length $\xi$ is longer in the viscoelastic case than the viscous case. Just as in the case of the passive filament, the effect of the length scale $\xi$ can be seen by comparing the viscous and viscoelastic cases. However, the wavelength $2\pi/k$ of the sliding force introduces another length scale. The combined presence of two different length scales can be seen, for example, in the shape of the hinged filament with De=0, and (dimensional) $k=8\pi/L$. In this example, $\xi$ is longer (and is the same as that seen for all the De=0 shapes of Fig. 5), while the shorter scale $2\pi/k$ leads to ripples on top of the longer deformation. Comparing the viscous to viscoelastic case, one can also see a decrease in the visible effects of the shorter lengthscale arising from the internal forces as $\xi$ increases and the shape is dominated by drag forces. For example, consider Fig. 6, which shows the effect of varying the Sperm number for an internal sliding

force with (dimensional) $k=8\pi/L$. As the Sperm number increases, $\xi$ decreases and smaller length-scale motions become more visible. One implication of the presence of these two length scales is that the observed "wavelength" of a beating pattern does not necessarily give direct information about either length scale.

The time-averaged power dissipated by the clamped and hinged internally driven filaments can be calculated as in the previous section, and is proportional to $\bar{f}_m^2$. The power versus De for a constant driving force, normalized by viscous power with $\lambda=0$, is shown in Figs. 7(a) and 7(b). Also shown for comparison is the power dissipated assuming that the beating shape of the viscous case is prescribed for the viscoelastic cases. For both prescribed forces and velocities, the growing imaginary component of the viscosity shifts the drag force to be out of phase with the velocity, decreasing the power dissipated. However, for large De the power dissipated for prescribed forces is always greater than that dissipated for prescribed velocities, because as De increases, the real part of the drag decreases in amplitude. Thus prescribed forces lead to motion with larger amplitude and velocity, and therefore more power dissipated relative to the case with prescribed velocities.
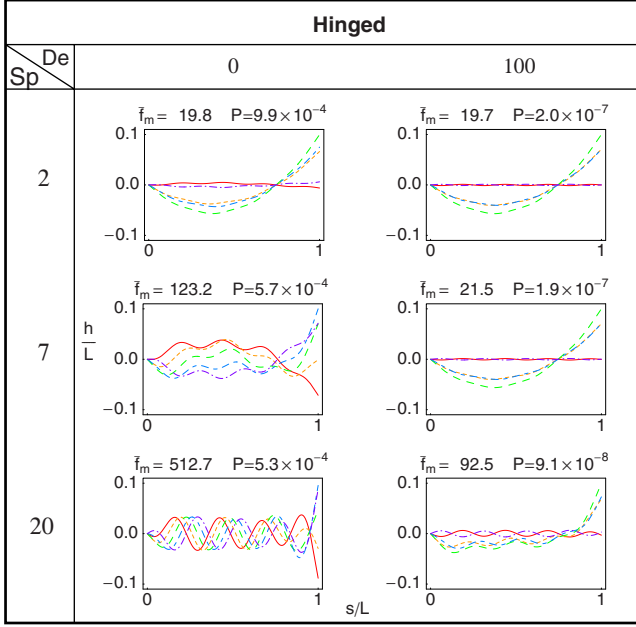
FIG. 6. (Color online) Shapes of beating patterns for hinged filaments with internal sliding forces, with varying Sp. A half cycle of the pattern is shown for viscous (De=0) and viscoelastic (De =100) cases, and for internal sliding forces given by Eq. (48) with $k/L=8\pi$. Time sequence: solid (red), short dash (orange), long dash (green), long dash-short dash (blue), dash-dot (purple). At the top of each figure, we print the (dimensionless) magnitude $\bar{f}_m$ required to produce motion with amplitude 0.1$L$, and the (dimensionless) power dissipated by the motion. The ratio of solvent viscosity to the total viscosity is $\eta_s/\eta=De_2/De=10^{-4}$.

### 2. Comparison to experimental beating patterns

The equation of motion for the active filament, Eq. (36), allows us to understand some of the qualitative changes in the shapes of beating patterns of sperm flagella in different media. There have been several studies observing the different beating patterns of sperm in media with increased viscosity and viscoelasticity [3–5]. Of these, we focus on the paper of Ishijima *et al.*, because it combines a systematic study of beating patterns in different media with measurements of viscosity using a falling-ball rheometer, and because its use of a pipette to hold the heads of observed sperm still makes its results amenable for modeling. In Fig. 8(a), the beating patterns of human sperm in Hanks' medium with viscosity of 1 cp, 35 cp, 4000 cp, and cervical mucus with viscosity 4360 cp are shown. The 35 cP and 4000 cP viscosity media are made by adding polyvinylpyrrolidone and methylcellulose, respectively, to Hanks' medium (a Newtonian solution of salts and glucose in water). As viscosity increases, motion is concentrated at the distal end, and motion in the proximal and middle portions of the flagella is damped out. Similar behavior was observed in Refs. [3,5].

At very high viscosity, asymptotic analysis of the equation of motion Eq. (36) demonstrates that most of the beating motion occurs at the end of the flagellum. For concreteness, because the beating patterns in Fig. 8(a) were obtained while the sperm head was held in place by a pipette, we use
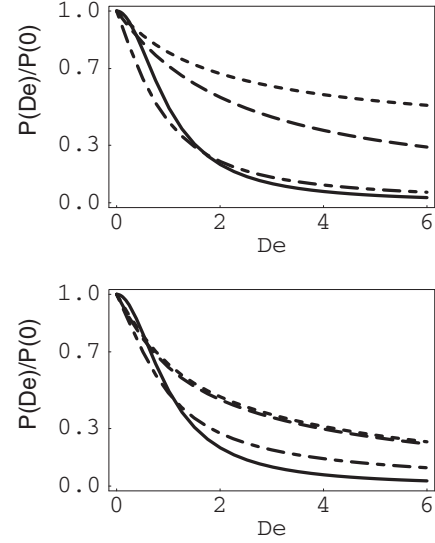


FIG. 7. Time-averaged power dissipated by filaments with active internal sliding forces, as a function of De=$\omega\lambda$. Power is normalized to the power dissipated in the viscous case De=0, with force amplitude such that maximum filament displacement in the viscous case De=0 is 0.1$L$. Different curves correspond to sliding forces given by Eq. (48) with different values of $k$: dashes, $k=0$; long dashes, $k=\pi/L$; long dash-short dash, $k=3\pi/L$. The solid curve is the power dissipated by a filament with a beating shape corresponding to the viscous case (De=0). In all cases, Sp=7. The ratio of solvent viscosity to the total viscosity is $\eta_s/\eta=De_2/De$ $=10^{-4}$. (a) Fixed head with clamped attachment point. (b) Fixed head with hinged attachment point.

clamped boundary conditions to model the motion. Furthermore, since wavelengths of 26–28 $\mu$m were observed in the low viscosity media for flagella of overall length $\approx$40 $\mu$m, we assume a sliding force with (nondimensional) $k=3\pi$ and the form of a traveling wave,

$$f_m(s) = \text{Re}\{\bar{f}_m e^{iks-it}\}. \quad (51)$$

Then the inhomogeneous part of Eq. (36) has the particular solution

$$h_p = ik\bar{f}_m e^{iks}/[-i\text{Sp}^4(1-i\text{De}_2)/(1-i\text{De})+k^4]. \quad (52)$$

while the homogeneous part $h_h(s)$ obeys

$$-i\text{Sp}^4\frac{1-i\text{De}_2}{1-i\text{De}}h_h + h_h'''' = 0, \quad (53)$$

with boundary conditions

$$h_h'''(1) = f_m(1) - h_p'''(1), \quad (54)$$

$$h_h''(1) = -h_p''(1), \quad (55)$$

$$h_h(0) = -h_p(0), \quad (56)$$

$$h_h'(0) = -h_p'(0). \quad (57)$$

We analyze the homogeneous solution by asymptotically matching solutions appropriate for the middle of the flagel-
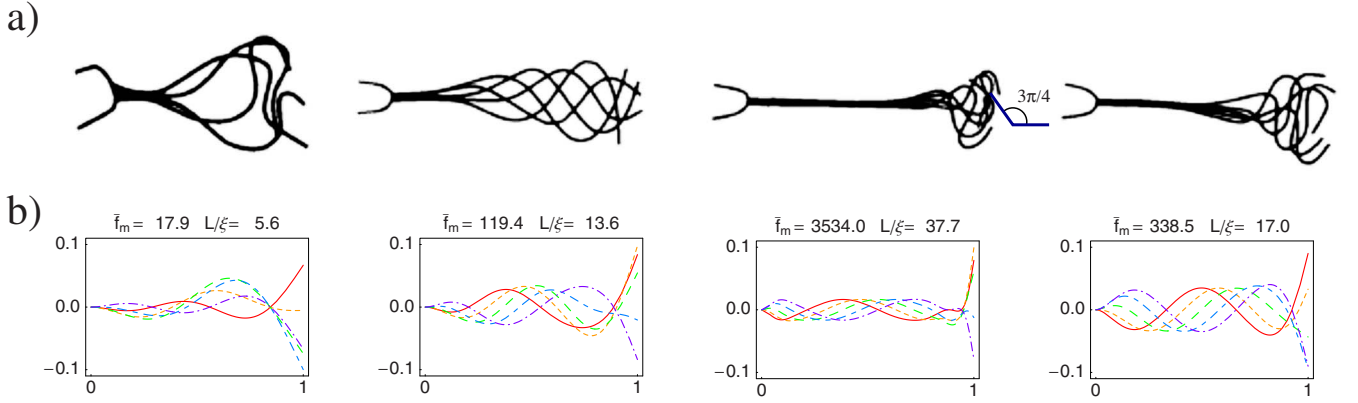
a)



b)



FIG. 8. (Color online) (a) Beating patterns of human sperm observed by Ishijima *et al.* [4] in (from left to right) 1 cP Hanks' solution, 35 cP Hanks' solution, 4000 cP Hanks' solution, 4360 cP cervical mucus. The sperm heads (on the left side of images) are held in place with a micropipette tip. The contour lengths of the flagella are approximately 40 $\mu$m. The thick (blue) line on the third panel indicates the maximum deflection angle $\theta(s)$. (b) Shapes of beating patterns for filaments with internal sliding forces, fixed head position, and clamped boundary conditions. A half cycle of the pattern is shown for internal sliding forces given by Eq. (51) with $k/L=3\pi$. Time sequence: solid (red), short dash (orange), long dash (green), long dash-short dash (blue), dash-dot (purple). From left to right, the sperm numbers are 5.6, 13.6, 37.7, and 45, corresponding to viscosities of 1 cP, 35 cP, 4000 cP, and 4360 cP. In the first two plots, the medium is purely viscous, while in the third plot, De=0.5 and $\text{De}_2$=0.5/4000. In the fourth plot, De=50 and $\text{De}_2$=50/4360. At the top of each figure, we print the (dimensionless) magnitude $\bar{f}_\mathrm{m}$ required to produce motion with amplitude 0.1L, and the length scale $\xi$.

lum with solutions appropriate for "boundary layers" at the ends of the flagellum. At high viscosity, the sperm number is large, and therefore the term involving the fourth power of the sperm number in Eq. (53) dominates. Throwing out the other terms, we find that the homogeneous solution vanishes. This balance is valid for the middle of the flagellum. But in a boundary layer near the ends of the flagellum, the homogeneous solution may vary rapidly, making the term with derivatives important. The size of this boundary layer can be expected to be of order $\xi=L|(1-i\text{De})/(1-i\text{De}_2)|^{1/4}/\text{Sp}$. Measuring lengths by $\xi$, i.e., $x=s/\xi$ for the proximal region, $x=(L-s)/\xi$ for the distal region, we obtain the equation of motion,

$$0 = -e^{i\theta}h_\mathrm{h} + \partial_x^4 h_\mathrm{h} \qquad (58)$$

$$e^{i\theta} = i\frac{1-i\text{De}_2}{1-i\text{De}}\left|\frac{1-i\text{De}}{1-i\text{De}_2}\right|. \qquad (59)$$

At the proximal end, the boundary conditions are

$$h_\mathrm{h}(x=0) = -h_\mathrm{p}(0), \qquad (60)$$

$$\partial_x h_\mathrm{h}(x=0) = -\partial_x h_\mathrm{p}(x=0), \qquad (61)$$

$$h_\mathrm{h}(x\to\infty) = 0, \qquad (62)$$

while at the distal end, the boundary conditions are

$$\partial_x^3 h_\mathrm{h}(x=0) = -\xi^3 f_\mathrm{m}(1) - \partial_x^3 h_\mathrm{p}(x=0), \qquad (63)$$

$$\partial_x^2 h_\mathrm{h}(x=0) = -\partial_x^2 h_\mathrm{p}(x=0), \qquad (64)$$

$$h_\mathrm{h}(x\to\infty) = 0. \qquad (65)$$

In the boundary conditions, the last constraint comes from the requirement that the solution in the boundary layers as-

ymptotically matches the solution in the middle of the flagellum. The solution to these equations is a linear combination of four exponential functions:

$$h_\mathrm{h}(x) = \sum_{n=0,1,2,3} c_n \exp(\rho_n x), \qquad (66)$$

$$\rho_n = \exp(i\theta/4 + in\pi/2). \qquad (67)$$

The $\rho_n$ have real and imaginary parts of similar order, so that the solutions decay or increase and have spatial oscillations on a similar length scale, which is approximately $\xi$ in dimensional units. Due to the asymptotic matching conditions, only the exponentials that decrease as $x$ increase are allowed, corresponding to $\rho_1$ and $\rho_2$ if $0 \leq \theta < 2\pi$.

At the proximal end, due to the clamped boundary conditions the homogeneous solution must cancel the inhomogeneous solution at the attachment to the head. The homogeneous solution is specified by

$$c_1 = \frac{-\rho_2 h_\mathrm{p}(0) + ikh_\mathrm{p}(0)}{\rho_2 - \rho_1}, \qquad (68)$$

$$c_2 = \frac{\rho_1 h_\mathrm{p}(0) - ikh_\mathrm{p}(0)}{\rho_2 - \rho_1}, \qquad (69)$$

which has an amplitude of order $f_\mathrm{m}(\xi/L)^4$, the same as the inhomogeneous solution. At the distal end, the largest term in the boundary conditions comes from balancing the sliding force. The homogeneous solution is specified by

$$c_1 = \frac{-\rho_2(ik)^2 h_\mathrm{p}(1) + [\xi^3 f_\mathrm{m}(1) + (ik)^3 h_\mathrm{p}(1)]}{\rho_1^2(\rho_2 - \rho_1)}, \qquad (70)$$

$$c_2 = \frac{\rho_1(ik)^2 h_\mathrm{p}(1) - [\xi^3 f_\mathrm{m}(1) + (ik)^3 h_\mathrm{p}(1)]}{\rho_2^2(\rho_2 - \rho_1)}, \qquad (71)$$

which has amplitude of order $f_\mathrm{m}(\xi/L)^3$. For high viscosities and low to moderate Deborah number this amplitude can be much larger than the amplitude of the proximal and inhomogeneous solutions. In the viscous case, with De=0, and high viscosity, the ratio between the amplitude of the homogeneous and inhomogeneous solution in the distal portion of the flagellum is of order $k/\mathrm{Sp}$.

To summarize, in the middle of the flagellum the homogeneous solution vanishes and the beating shape is dominated by the inhomogeneous solution, which has a magnitude which decreases as viscosity increases, and is small for high viscosity. At the proximal end of the flagellum, the homogeneous solution is of the same order as the inhomogeneous solution due to the clamped boundary conditions. On the other hand, the motion at the distal end is dominated by the homogeneous solution, has larger amplitude than the middle portion, decays exponentially with a length scale $\xi$, and can have oscillations with wavelengths up to a few times smaller than $\xi$. Thus in high viscosity solutions the motion of flagellar beating patterns are constrained to the distal tip. Although we assume only a single mode of the sliding force, the asymptotic analysis is generally valid, and should also apply to more realistic sliding forces.

In Fig. 8(b) we plot flagellar beating patterns for a sliding force of $k=3\pi/L$. We constrain the motion to lie in a two-dimensional plane for simplicity, although the observed beating patterns are three dimensional. These beating patterns are obtained by solving the linear Eq. (36) exactly, i.e., not using the asymptotic analysis. In this modeling we assume the pure Hanks' solution and Hanks' solution with polyvinylpyrrolidone to be Newtonian. For the Hanks' solution with methylcellulose we assume a Deborah number of 0.5, corresponding to a beating frequency of 7 Hz [4] and a relaxation time constant of about $10^{-2}$ s [24]. For the cervical mucus we assume a Deborah number of 50, corresponding to a beating frequency of 12 Hz [4] and a relaxation time constant of a little less than a second [25]. To determine $\mathrm{De}_2$ we use the ratio $\eta_s/\eta = 1 \text{ cP}/4360 \text{ cP}$. The sperm numbers are determined from $L=40 \ \mu m$, $\zeta_\perp = 2\eta$, $A=4\times10^{-22}$ Nm$^2$ [11], viscosities from Fig. 8 and frequencies of 12 Hz for the 1 cP and 35 cP media, 7 Hz for the 4000 cP media, and 12 Hz for cervical mucus [4].

In the plots, the amplitude of the beating pattern is proportional to the driving force $\widetilde{f}_\mathrm{m}$. The amplitude in the middle sections is therefore nearly completely suppressed as viscosity increases as compared to the amplitude in the 1 cP case. At the same time, the motion near the end of the flagellum is relatively unsuppressed. In addition, the observed beating pattern in cervical mucus has motion extending farther away from the distal end than the beating pattern in 4000 cP Hanks' solution, in both the experimental [Fig. 8(a)] and modeled [Fig. 8(b)] beating patterns. This agrees with the fact that the length scale $\xi$ decreases as viscoelastic effects become important.

Finally, in Fig. 9, we plot the result from the asymptotic analysis for parameters corresponding to the third case of
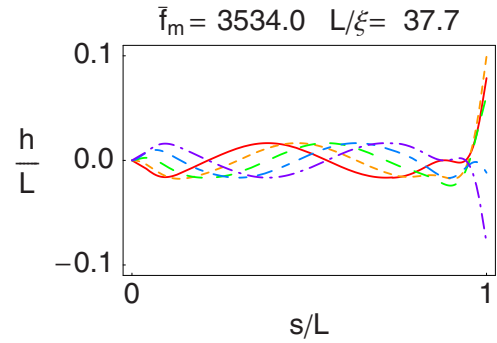


FIG. 9. (Color online) Shape of beating pattern for filament with internal sliding forces, fixed head position, and clamped boundary conditions obtained from asymptotic analysis. A half cycle of the pattern is shown for internal sliding forces given by Eq. (51) with $k/L=3\pi$. Time sequence: solid (red), short dash (orange), long dash (green), long dash-short dash (blue), dash-dot (purple). The sperm number is 37.7, corresponding to a viscosity of 4000 cP, and De =0.5, while $\mathrm{De}_2=0.5/4000$. At the top of the figure, we print the (dimensionless) magnitude $\bar{f}_\mathrm{m}$ required to produce motion with amplitude $0.1L$, and the lengthscale $\xi$.

Fig. 8 (4000 cP Hanks' solution). The asymptotic solution matches the exact solution quite well.

## VI. DISCUSSION

In a viscoelastic medium the forces exerted on a flexible swimmer are different from those exerted by a Newtonian medium. We have calculated the viscoelastic forces for a medium with fading memory using resistive force theory. The effects of hydrodynamic forces on flexible swimmers can be seen in the passive filament model we have described. We have also used a simple model of an active filament to shed some light on the motion of sperm flagella in different media.

In agreement with experimental observations, the sliding filament model shows that the beating is confined to the distal tip for the high viscosity Hanks' solution. While the experimental beating patterns are qualitatively explained by the high-viscosity asymptotic analysis, and the solutions in Fig. 8(b) show the same qualitative trends, our model is not quantitatively accurate. For example, in the cervical mucus, our model shows much less confinement of motion to the distal tip than the observed beating patterns. In particular, we note that according to our model, only the third panel of Fig. 8(b) is in the strongly asymptotic regime, in contrast to the beating patterns of Ishijima *et al.*, in which the motion in cervical mucus also seems to be in the asymptotic regime. The discrepancy between our models and the observed beating patterns may be due to an overestimation of the Deborah number, or our approximation of small amplitudes. The actual beating patterns show large amplitudes and curvatures; for example, the maximum deflection angle shown in Fig. 8(a) corresponds to a sliding amplitude $\Delta(s)=-3a\pi/4 \approx -2.4a$. Another source of discrepancy is our use of a simple form of the sliding force. Ishijima *et al.* observe varying beating frequencies in different media, indicating that the sliding force

itself is changing in response to the different drag forces exerted in different media. Changes in the active force due to changes in the media have been modeled by various workers [12,26,27]. We have specified a fixed force; however, our analysis might be useful in extending studies of the sliding mechanism such as in Ref. [12] to high viscosity and viscoelastic situations. Finally, our simple model does not take into account the possibility of non-Newtonian behavior which extends beyond viscoelasticity in Hanks' medium with added polymers. We note that in the case of methylcellulose solutions, the swimming of bacteria with helical flagella has been analyzed by introducing different viscosities for parallel and perpendicular drag coefficients [28]. This type of treatment would not affect our results, since at first order the shape is determined solely by the perpendicular drag component in our model. However, the work of Ref. [28] points out that care should be taken to measure appropriate viscosities for flagellar movements, especially as the viscosity of methycellulose solutions is known to be shear-rate dependent.

Our work is a first step to understanding how swimming is modified in a complex medium. There is scope to expand these studies, probably numerically, in addressing questions such as the role of end effects and associated elongational flows, the role of drag from a head and the role of large amplitude motion in viscolastic fluids. In addition, many biological media, including mucus in the reproductive tract, are gels, which may be expected to have different effects on the swimming than fluids.

### APPENDIX: PROBLEMS WITH APPLYING LINEAR VISCOELASTIC CONSTITUTIVE RELATIONS TO SWIMMING VELOCITY

We have seen that both the leading-order shape of a beating filament and the power dissipated by a filament are determined by the linearized form of the nonlinear constitutive relation (18),

$$\boldsymbol{\tau} + \lambda \dot{\boldsymbol{\tau}} = \eta \dot{\boldsymbol{\gamma}} + \lambda \eta_s \ddot{\boldsymbol{\gamma}}. \qquad (A1)$$

We have also noted that for the linear constitutive relation (A1) with $\eta_s = 0$, the swimming speed of a filament with prescribed shape is the same as the speed for a filament in a Newtonian fluid [16]. Finally, we have emphasized that since the leading-order form of the swimming velocity is quadratic in the deflection of the filament, the use of Eq. (A1) to calculate swimming velocity fails to capture leading-order terms arising from the full nonlinear constitutive relation [15,17]. In this Appendix, we show that the use of Eq. (A1) to calculate a swimming speed not only misses important leading-order contributions, but also leads to inconsistent results.
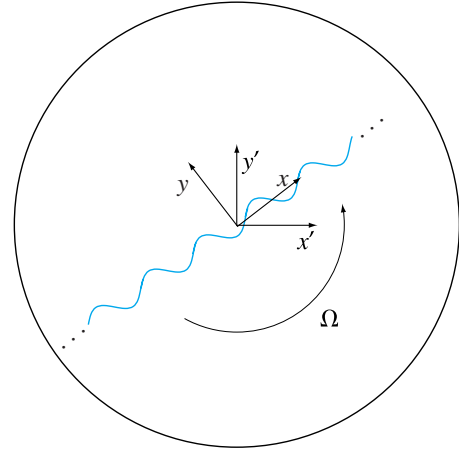


FIG. 10. (Color online) Infinite filament in a viscoelastic medium on a table rotating with angular speed $\Omega$. The coordinates $\{x, y\}$ rotate with the table; $\{x', y'\}$ are space fixed.

The origin of the inconsistency is the fact that linear viscoelastic models are inapplicable when displacement gradients become large. The classic illustration is the case of a shear flow in a channel on a slowly rotating table [6]. If the rotation rate is small enough that fictitious forces such as the centrifugal and Coriolis forces are negligible compared to the viscous forces acting on the polymers in solution, then the zero-frequency shear modulus $\eta_0$ must be independent of the rotation speed $\Omega$. A short calculation shows that Eq. (A1) predicts that $\eta_0$, calculated in the rotating frame, depends on $\Omega$, an unphysical result [6].

Now consider a swimmer in a medium governed by Eq. (A1). To simplify the algebra, we consider an infinitely long active filament with no resistance to bending, $A = 0$, or Sp $\rightarrow \infty$. The sliding force has the traveling wave form of Eq. (48). The swimmer and the medium are on a table that rotates with angular speed $\Omega$ (Fig. 10). Since $\Omega$ is small enough to make fictitious forces negligible, the swimming speed $U$ in the body-fixed frame $\{\hat{\mathbf{e}}_x, \hat{\mathbf{e}}_y\}$ cannot depend on $\Omega$ and must be the same as the swimming speed in the absence of rotation.

The resistive force theory corresponding to Eq. (A1) is Eq. (24). The components of the forces in the body-fixed frame obey

$$\lambda(\dot{f}_x - \Omega f_y) + f_x = -\zeta_\parallel U - (\zeta_\perp - \zeta_\parallel)\partial_x h \partial_t h, \qquad (A2)$$

$$\lambda(\dot{f}_y + \Omega f_x) + f_y = \zeta_\perp \partial_t h. \qquad (A3)$$

Just as in our analysis in the main text, the force $\mathbf{f}$ from the medium balances the internal force on the filament: $\mathbf{f} + \mathbf{f}_{int} = 0$. In the limit of vanishing bending stiffness,

$$\mathbf{f}_{int} = -a\partial_x f_m \hat{\mathbf{e}}_y. \qquad (A4)$$

Examination of the spatial average of Eq. (A2) shows that the swimming velocity vanishes to first order in deflection, $U^{(1)} = 0$. To second order, Eq. (A2) implies

$$U^{(2)} = -\frac{\zeta_\perp - \zeta_\parallel}{\zeta_\parallel}\langle\partial_x h\partial_t h\rangle. \tag{A5}$$

Thus, to find the swimming velocity, we must solve Eqs. (A2) and (A3) for the first order deflection,

$$\widetilde{h} = -\frac{(1 - i\mathrm{De})^2 + \lambda^2\Omega^2}{1 - i\mathrm{De}}\frac{ak\widetilde{f}_{\mathrm{m}}}{\zeta_\perp\omega}. \tag{A6}$$

Using this expression in Eq. (A5) leads to

$$U^{(2)} = \frac{k\omega}{2}\frac{\zeta_\perp - \zeta_\parallel}{\zeta_\parallel}\frac{(1 + \lambda^2\Omega^2 - \mathrm{De}^2)^2 + 4\mathrm{De}^2}{1 + \mathrm{De}^2}\frac{a^2 k^2 |\bar{f}_{\mathrm{m}}|^2}{\zeta_\perp^2\omega^2}. \tag{A7}$$

Linear resistive force theory predicts that the swimming velocity of an active filament on a rotating turntable depends on the rate of rotation of the turntable. This result is unphysical, and leads to the conclusion that linearly viscoelastic constitutive relations should not be applied to the swimming problem.

[1] D. Bray, *Cell Movements: From Molecules to Motility*, 2nd edition (Garland Publishing, Inc., New York, 2001).

[2] *Cilia and Flagella*, edited by M. A. Sleigh (Academic Press, London 1974).

[3] R. Rikmenspoel, J. Exp. Biol. **108**, 205 (1984).

[4] S. Ishijima, S. Oshio, and H. Mohri, Gamete Res. **13**, 185 (1986).

[5] S. Suarez and X. Dai, Biol. Reprod. **46**, 686 (1992).

[6] R. B. Bird, R. C. Armstrong, and O. Hassager, *Dynamics of Polymeric Liquids*, Fluid Mechanics Vol. 1 (Wiley, New York, 1977).

[7] K. E. Machin, J. Exp. Biol. **35**, 796 (1958).

[8] C. H. Wiggins and R. E. Goldstein, Phys. Rev. Lett. **80**, 3879 (1998).

[9] T. S. Yu, E. Lauga, and A. E. Hosoi, Phys. Fluids **18**, 091701 (2006).

[10] E. Lauga, Phys. Rev. E **75**, 041916 (2007).

[11] S. Camalet, F. Jülicher, and J. Prost, Phys. Rev. Lett. **82**, 1590 (1999).

[12] I. H. Riedel-Kruse, A. Hilfinger, J. Howard, and F. Julicher, HFSP J. **1**, 192 (2007).

[13] S. Suarez, D. Katz, D. Owen, J. Andrew, and R. Powell, Natl. Med. Leg J. **44**, 375 (1991).

[14] H. Ho and S. S. Suarez, Reprod. Dom. Anim. **38**, 119 (2003).

[15] H. C. Fu, T. R. Powers, and C. W. Wolgemuth, Phys. Rev. Lett. **99**, 258101 (2007).

[16] G. R. Fulford, D. F. Katz, and R. L. Powell, Biorheology **35**, 295 (1998).

[17] E. Lauga, Phys. Fluids **19**, 083104 (2007).

[18] L. D. Landau and E. M. Lifshitz, *Theory of Elasticity*, 3rd edition (Pergamon Press, Oxford, 1986).

[19] S. Camalet and F. Jülicher, New J. Phys. **2**, 24.1 (2000).

[20] J. Gray and G. J. Hancock, J. Exp. Biol. **32**, 802 (1955).

[21] S. A. Koehler and T. R. Powers, Phys. Rev. Lett. **85**, 4827 (2000).

[22] B. Qian, T. R. Powers, and K. S. Breuer, Phys. Rev. Lett. **100**, 078101 (2008).

[23] H. C. Fu, T. R. Powers, and C. W. Wolgemuth (unpublished).

[24] T. Amari and M. Nakamura, J. Appl. Polym. Sci. **17**, 589 (1973).

[25] P. Y. Tam, D. F. Katz, and S. A. Berger, Biorheology **17**, 465 (1980).

[26] C. J. Brokaw, J. Exp. Biol. **55**, 289 (1971).

[27] C. Lindemann, J. Theor. Biol. **168**, 175 (1994).

[28] Y. Magariyama and S. Kudo, Biophys. J. **83**, 733 (2002).